The 2.7 Å Crystal Structure of the Activated FERM Domain of Moesin: An Analysis of Structural Changes on Activation[†,‡]

Simon D. Edwards and Nicholas H. Keep*

BBSRC Bloomsbury Centre for Structural Biology and School of Crystallography, Birkbeck College, University of London, Malet Street, London WC1E 7HX, U.K.

Received February 28, 2001; Revised Manuscript Received April 24, 2001

ABSTRACT: Moesin binds to a large range of proteins through its N terminal FERM (band 4.1, ezrin, radixin, moesin) domain. In full-length moesin isolated from cells, this binding is masked by binding to the C-terminal domain of moesin (C-ERMAD). Activation takes place by phosphorylation of Thr 558 in the C-ERMAD, which releases the C-ERMAD. A recently determined crystal structure of a noncovalent complex of the FERM and C-ERMAD domains showed for the first time that the structure of the FERM domain consists of three subdomains, each of which is similar to known structures. The structure reported here also contains a unique 47-residue helix pointing away from the FERM domain at the start of the α domain, in agreement with secondary structure predictions. Removal of the C-ERMAD does not result in a huge rearrangement of the FERM domain, but comparison with the activated radixin structure shows a consistent set of small changes. Not surprisingly, the exposed C-ERMAD binding area interacts in crystal contacts. More interestingly, a negatively charged peptide binds to the inositol site in a crystal contact and causes a greater conformational change in the structure than inositol.

The ERM[1] (ezrin/radixin/moesin) family of proteins form one of the physical links between the plasma membrane and the actin cytoskeleton. Experiments for determining the localization of the ERM proteins have found them to be concentrated in actin-rich membrane structures such as microspikes, microvilli, and membrane ruffles close to the plasma membrane (for recent reviews, see refs *1*−*3*).

The sequences of ezrin (*4*), radixin (*5*), and moesin (*6*) are nearly identical to each other; murine ezrin, radixin, and moesin have sequence identity of 75, 82, and 80% respectively (*3*). Neurofibromatosis tumor suppressor 2 (NF2), also known as merlin, is homologous to the ERM proteins throughout most of its length (*7*) and can dimerize with ERM proteins. An inherited mutation in merlin leads to a range of central nervous system tumors when a second mutation is acquired in a cell lineage (*8*). The sequence of the N-terminus of the ERM proteins is homologous to the first ∼300 residues of the erythrocyte band 4.1 protein, which connects the actin/spectrin network to the membrane protein glycophorin C (*9*). This motif has been called the FERM domain (*10*) and is also found in talin, some protein tyrosine phosphatases, some non-muscle myosins, and FAK and JAK kinases (*11*).

After the ∼300-residue N-terminal FERM domain, all the ERM proteins have an ∼200-residue region that is predicted to be largely α-helical and a C-terminal tail domain of ∼100 residues (*12*). F-Actin binds to the last 34 residues at the C-terminus (*13*). An internal actin-binding site has been found corresponding to residues 280−333 by a solid phase assay (*14*) or 280−310 by a cell extension assay (*15*). They also found a requirement for the first 29 amino acids at the N-terminus. This can be interpreted as a requirement for a fully folded FERM domain as the smaller constructs that do not bind actin have residues from the main domain missing. However, there are examples such as utrophin (*16*, *17*) where charged sequences adjacent to a folded domain enhance the binding affinity for actin.

The ERM proteins are isolated in a "dormant" state in which the biologically relevant binding sites are conformationaly masked by association of the amino-terminal (residues 1−296) FERM (also known as the N-ERMAD) domain and carboxy-terminal (residues 479−585) regions (C-ERMAD) (*18*). Both self-association within a monomer and head-to-tail homo- and heterodimers of ERM proteins have been observed (Figure 1). Activation of the C-ERMAD for binding to actin requires separation from the FERM domain. This is achieved by phosphorylation of Thr 558 (*19*, *20*).

There are a number of binding partners of the ERM family which interact with the FERM domain. These can be divided into three groups. The first group includes the hyaluronan receptor (CD44) (*21*), leukosialin, CD43, and ICAM-1, -2, and -3 (*22*). These interact with the FERM domain via a basic region immediately on the cytoplasmic side of the single transmembrane helix. This sequence has been most clearly defined for CD44 (*22*, *23*). These may be

[†] Funded by an MRC Studentship to S.D.E. and a Royal Society Project Grant to N.H.K.

[‡] Coordinates and structure factors for the moesin FERM domain are deposited in the Protein Data Bank as entry 1E5W.

* Corresponding author. E-mail: n.keep@mail.cryst.bbk.ac.uk. Telephone: 020-7631-6852. Fax: 020-7631-6803.

[1] Abbreviations: C-ERMAD, C-terminal ERM protein association domain; EMBL, European Molecular Biology Laboratory; ERM, ezrin, radixin, moesin family of proteins; FERM, 4.1, ezrin, radixin, moesin homology domain; IP3, inositol 1,4,5-trisphosphate; NF2, neurofibromatosis tumor suppressor 2; PIP2, phosphatidylinositol 4,5-bisphosphate; rmsd, root mean square deviation; SRS, Synchrotron Radiation Source.

10.1021/bi010419h CCC: $20.00
Published on Web 05/19/2001

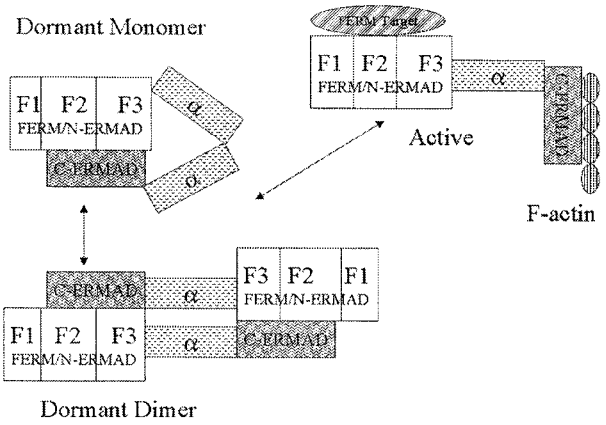

FIGURE 1: Modes of association of the ERM family protein domains. In the dormant form, the FERM domain binds to the C-ERMAD. This can be as a monomer or dimer. On activation, the domains separate and can bind to their targets.

able to bind in the presence of the C-ERMAD, and the binding is enhanced by phosphoinositides (*24*−*26*).

In the second group are E3KARP and EBP50 which are related proteins that bind to the Na^+/H^+ exchanger of the kidney proximal tubule and to the FERM domain (*27*, *28*). A number of other membrane proteins also bind to this group. These proteins and the ERM proteins act together to form a two-stage linker between the membrane and the cytoskeleton.

A final group consists of a number of regulators of signal transduction. These include the regulatory subunit of phosphatidylinositol 3-kinase p85 (*29*), rho-GDI (GDP dissociation inhibitor), a regulator of the rho family of small G proteins which regulate various actin-based cellular events (*25*, *30*), Dbl, a G protein exchange factor (*31*), and the myosin binding subunit of myosin phosphatase (*32*). Some of these are reported only to bind to the isolated FERM domain and others also to the full-length (and presumably dormant) protein, but all require the FERM domain to be present.

Here we report the 2.7 Å structure of the moesin FERM domain and the start of the α domain in an "activated" form without the C-ERMAD bound. We compare it to the dormant FERM domain/C-ERMAD structure (*33*) and to the FERM domain of radixin (*34*).

MATERIALS AND METHODS

Protein Purification, Crystallization, and Data Collection. Moesin (residues 1−346) was expressed in *Escherichia coli* as a nonfusion protein using a derivative of the pET28a (Novagen, Madison, WI) T7-based expression plasmid lacking the His tag. It was purified by anion exchange chromatography (Fast Flow S, Pharmacia) followed by gel filtration (S200 Sephadex, Pharmacia) in 20 mM Tris, 150 mM NaCl, and 1 mM DTT (pH 7.5). Crystals grew by hanging drop vapor diffusion at 16 °C. Two microliters of 10−15 mg/mL protein was mixed with 2 μL of mother liquor consisting of 100 mM Hepes (pH 7.5) and 25% ethylene glycol on a siliconized glass coverslip and equilibrated against 1 mL of mother liquor. Crystals were transferred into a cryoprotective solution of 100 mM Hepes, 25% ethylene glycol, and 15% glycerol and flash-frozen in liquid nitrogen. MAD data were collected using four wavelengths off the same crystal at 100 K [0.9774 (peak) and 1.300 Å (low-energy remote) on station PX9.5 at SRS Daresbury (Warrington, U.K.); 0.9796 (inflection) and 0.9686 Å (high-energy remote) at BW7A at EMBL Hamburg (Hamburg, Germany)]. A native data set for a methionine-containing crystal was collected on SRS station PX9.6 at 100 K using a wavelength of 0.87 Å to 2.7 Å resolution. Data were processed using MOSFLM (*35*), and intensities were scaled using SCALA (*36*, *37*).

Structure Solution and Refinement. Methionine sites were found in the MAD data using SOLVE (*38*). Site refinement, phase calculations, and solvent flattening were performed in SHARP (*39*). An initial model was built into the resulting 3.5 Å map with the program O (*40*) using the selenium sites to keep the structure in register (Table 1).

This was then refined against data from a methionine-containing crystal at 2.7 Å using CNS (*41*) by rounds of refinement and manual model rebuilding using O. Toward the end of the refinement, water atoms were added by visual inspection in difference density where there was a likely H bond donor or acceptor. Those sites that refined with a relatively low *B* factor were retained. The final refinement statistics are listed in Table 2.

Structure Analysis. Structural superpositions and calculations were carried out using the Swiss PDB viewer (*42*) (http://www.expasy.ch/spdbv). Domain movements were analyzed with DYNDOM (*43*). Merlin mutations were obtained from a paper (*12*), from the HGMD database (http://archive.uwcm.ac.uk/uwcm/mg/hgmd0.html) (*44*) and from a Web site (http://neuro-trials1.mgh.harvard.edu/nf2/). A model of the FERM domain and first α-helix of merlin was constructed using the Swiss-Model programs (*42*). The 25 point mutations or single amino acid insertions and/or deletions were examined.

RESULTS

Structure Determination and Description. The protein forms bipyramidal crystals in space group $P4_22_12$. The crystals show poor isomorphism, varying particularly in cell length *c*. The structure was phased by selenomethionine multiwavelength anomalous dispersion from a single crystal to 3.5 Å (Table 1). There are 10 methionines in the protein, and nine sites were found by SOLVE (*38*), indicating one molecule per asymmetric unit and a solvent content of 66%. Only nine sites were found as methionine residues 318 and 322 from symmetry-related molecules are close (5.1 Å Se−Se distance) so that the sites were not resolved by SOLVE. Refinement was carried out against data from a methionine-containing crystal to 2.7 Å (Table 2). The final refined model contains all residues (1−346) in the crystallized moesin construct and 36 water molecules.

Recently, a number of structures of FERM domain proteins have been published. These are the dormant complex of the moesin FERM domain (residues 1−297; residues 4−297 observed) with the C-ERMAD (residues 467−577; residues 488−577 observed) (PDB entry 1EF1) (*33*), the activated complex of radixin (residues 1−310; residues 1−297 observed) with and without the activator inositol 1,4,5-trisphosphate (IP3) (PDB entries 1GC6 and 1GC7) (*34*), and the protein 4.1 core domain (residues 1−279 observed) (PDB

Table 1: Selenomethionine in Crystal Space Group $P4_22_12$ ($a = b = 95.36$ Å and $c = 152.9$ Å)

	SRS 9.5	BW7A	SRS 9.5	BW7A
data set	λ_1 (1.300), high-energy remote	λ_2 (0.9796), point of inflection	λ_3 (0.9774), peak	λ_4 (0.9686), low-energy remote
resolution range (Å) (final shell)	76−3.5 (3.69−3.5)	41−3.5 (3.69−3.5)	67−3.5 (3.69−3.5)	40−3.5 (3.69−3.5)
no. of unique reflections	9345	9573	9347	9277
completeness (final shell)	99.6 (99.6)	99.5 (99.5)	99.7 (99.7)	99.6 (99.6)
redundancy (final shell)	14.3 (14.7)	7.8 (8.1)	11.5 (11.8)	7.8 (8.0)
anomalous completeness	99.9	99.5	99.9	99.6
R_{merge} (final shell)	0.068 (0.375)	0.048 (0.227)	0.068 (0.378)	0.046 (0.202)
R_{anom} (final shell)	0.021 (0.099)	0.024 (0.082)	0.045 (0.114)	0.040 (0.075)
phasing power (SHARP)				
isomorphous centric (acentric)		1.4 (3.2)	1.5 (3.4)	1.3 (2.4)
anomalous	1.4	2.6	3.0	3.6
figure of merit (SHARP) (before/after solvent flattening)	0.76/0.86			

Table 2: Native Crystal in Space Group $P4_22_12$ ($a = b = 94.35$ Å and $c = 156.1$ Å)

	all data	highest-resolution shell
Data Collection		
resolution (Å)	37−2.70	2.85−2.70
no. of observations	110406	15646
no. of reflections	19994	2805
completeness (%)	99.7	99.9
redundancy	5.5	5.5
I/σ	4.6	3.0
R_{merge}	0.046	0.246
Refinement		
resolution (Å)	37−2.70	2.87−2.70
no. of refined observations	18965	3077
no. of free observations (5%)	1019	160
R-factor (%)	25.3	42.5
R_{free} (%)	29.3	45.5
Model		
no. of atoms	2924 proteins, 36 waters	
rmsd for bond lengths (Å)	0.007	
rmsd for bond angles (deg)	1.3	
chain	all	
average B (Å^2)	74.0	
main chain B (Å^2)	70.4	
side chain and water B (Å^2)	77.3	
Wilson B (Å^2) from TRUNCATE	89.3	

entry 1GG3) (*45*). Moesin and radixin are 90% identical in the region of residues 1−297 and are probably isoforms with similar function. Protein 4.1 is much more distantly related with only a sequence identity of 16.5% in the structural alignment with moesin. Nevertheless, the overall fold is preserved with the rmsd of the Cα superposition being less than 2.0 Å for any pair of structures with 258 amino acids included. The radixin structures with and without IP3 show an Cα rmsd of only 0.3 Å and so give identical results in the analyses. Only the IP3-bound structure is shown in the figures.

The unique feature of our structure is the 49 C-terminal residues, which form an extended helix. This agrees with secondary structure predictions of the ERM family (*12*). The rest of the structure is very similar to the other ERM family structures (Figure 2). As previously observed (*33*−*35*), the fold consists of three domains arranged in a trefoil each showing similarity to known structures. Briefly, the first module, F1 (residues 5−82), contains a five-stranded β-sheet with an α-helix running across it. This module has a structure similar to ubiquitin (*46*). The next module, F2 (residues 96−195), is entirely α-helical with a short linker region of 30 residues between the second and third of four helices. This shows similarity to acyl-CoA binding protein (*47*). The final module in the FERM domain, F3 (residue 204−296), is comprised of a sandwich of two orthogonal antiparallel β-sheets followed by an α-helix. The fold is found in a number of domain families, including phosphotyrosine binding (PTB), pleckstrin homology (PH), and enabled/VASP homology 1 (EVH1) domains (*48*). In all cases, the FERM domains are more similar to each other than to the other structurally related domains.

Analysis of Structural Changes. Although the activation of the FERM domain by removal of the C-ERMAD does not cause a large change in the structure, it is important to see what effect it has. The rmsd on alignment of the dormant and activated moesin structures is greater (2.0 Å for 294 Cα residues) than the average of superimposing the three domains (Cα rmsd for residues 4−90, 91−200, and 201−297 of 1.1 Å). The regions that differ most between the dormant and active moesin are residues 19−23, 51−55, 71−75, 139−145, 162−171, 211−216, and 260−265 (most residues in these regions have Cα−Cα distances of >3.0 Å) (Figures 2 and 3). These are similar to the regions that differ between dormant moesin and active radixin (*34*). In particular, the active radixin and moesin structures superimpose with each other much better in the region of residues 139−145, 163−167, and 260−265 than with the dormant moesin (Figure 3).

An alternative analysis of structural displacement is implemented in Dyndom (*43*), which looks for concerted movements of regions of the protein. This analyzes the difference between dormant and active moesin as the C-terminal half (residues 241−282) of F3 rotates by 16.7° with a ratio of interdomain to intradomain movement of 1.25. A similar region also moves in the activated structure of radixin relative to dormant moesin, but around a somewhat different axis. The possible biological relevance of these differences is presented in the Discussion.

Crystal Contacts. Unlike enzyme active sites that tend to be in the interior of a protein molecule, protein−protein interaction sites are usually on the surface and therefore changes observed between crystal structures of a molecule by itself and in a complex may well be in part due to crystal contacts. Crystal contacts can cause changes in structure of the size being discussed above. Therefore, the crystal contacts seen in the active moesin construct are listed below.

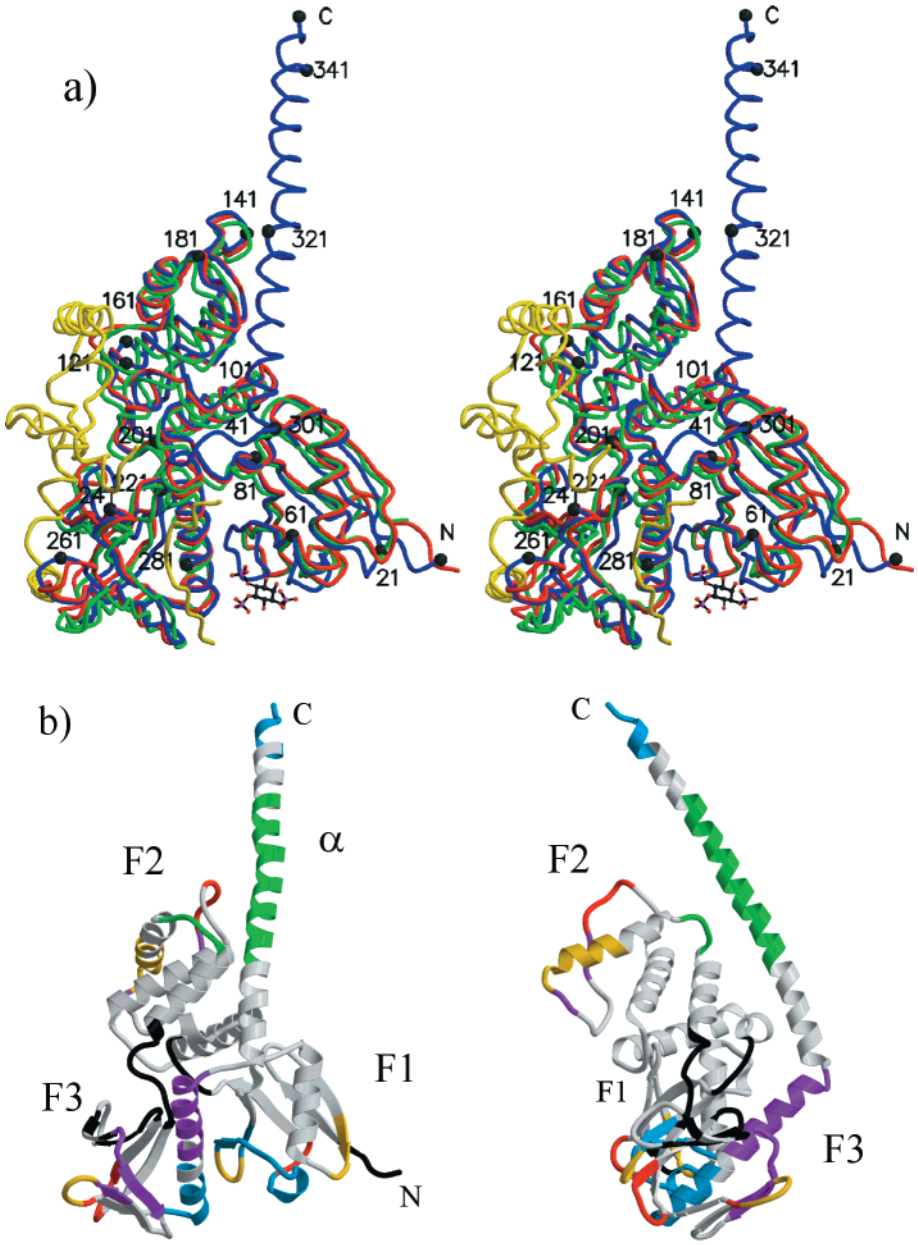

FIGURE 2: Overall structure and superposition of the FERM domain. (a) Stereopair of the superposition of the Cα atoms of our activated FERM domain structure (blue) (PDB entry 1E5W) on the dormant FERM domain structure (green) and the C-ERMAD (yellow) (*33*) (PDB entry 1EF1) and on the IP3-bound radixin (red) (PDB entry 1GC6) (*34*). Superposition performed using Swiss PDB viewer (*42*). Figure drawn with MOLSCRIPT (*57*) and Raster3D (*58*). (b) Secondary structure cartoon of the activated mosein structure colored to show crystal contacts. These are green, black, cyan, and purple in the order discussed in the text. Regions where the Cα carbons are more than 3 Å from the dormant moesin are in red or where they overlap with crystal contacts in yellow.

Unusually, both the N- and C-termini are ordered due to crystal contacts.

Seven symmetry-related molecules contact moesin residues 1−346. These form four different types of contacts (Figure 2b). One is symmetric and hence the odd number of contacting moesins; residues 314−332 in the long C-terminal helix contact the equivalent region in a second molecule. In the second contact type, the N-terminus is inserted toward the core of the FERM domain so that it contacts both the linkers between F1 and F2 (residues 85−87) and between F2 and F3 (residues 196−203) and parts of F3 (residues 221−228). In the third type of crystal contact, the negatively charged residues and the C-terminal carboxyl of the C-terminus (342-REKEE-346) interact with a positively charged patch at the start of the helix of module F3 (R275, K278, and R279) and K60 and K63 of module F1. In the fourth type, residues 148 and 159−166 in F2 contact residues 242−248, 258−263, and 285−296 in F3. As shown in Figure 2b, some but not all the regions that have moved most from the dormant moesin structure are involved in crystal contacts.

Pathogenic Mutations in Merlin. Twenty-five point or single amino acid insertion and/or deletion mutations were identified from the literature (Figure 4). These were examined on a homology model. Most mutations resulted in a clear disruption of the hydrophobic core or secondary structure elements. Some were hard to explain and may be polymorphisms [M77V, E106G (not a conserved site in the ERM family), and R351H]. A few could be interpreted in terms of interactions discussed in this paper and are mentioned at the appropriate point in the Discussion.

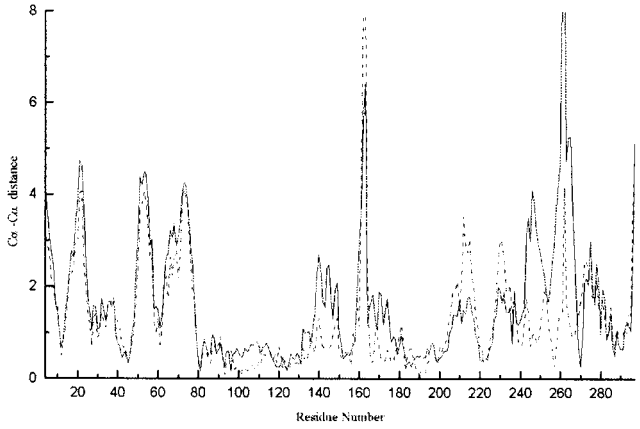

FIGURE 3: Plot of Cα−Cα distances in the superimposed molecules plotted vs residue number. The plot of dormant moesin vs active moesin is in solid lines and that of active moesin vs IP3-bound radixin in dotted lines. Superpositions done in PDB Viewer and distances calcuated in LSQMAN (*59*).

DISCUSSION

Extended Helix at the Start of the α*-Domain.* Uniquely, our structure continues for some 50 residues after the end of the FERM domain. This is a single long helix in line with secondary structure predictions for this region (*12*). The helix makes limited contacts with the FERM domain. Q308 makes a side chain−side chain hydrogen bond to R40. M305 is in a hydrophobic pocket between residues 40 and 41 and residues 94 and 95 of the FERM domain. The side chain of T299 makes hydrogen bonds to residue 301 and 302 main chain N, T299 main chain O hydrogen bonds to the Q303 side chain, and E298 makes a side chain hydrogen bond to K306. All these residues are identical in the ERM family and highly conserved (T299S and I300L) in merlin. The higher level of sequence conservation of the FERM domain of the ERM proteins, compared to the rest of the protein, continues past the end of the domain to residue ∼308. It is likely then that the angle of the helix to the domain is conserved. This is also supported by a number of pathogenic mutants of merlin. S315F, which is the merlin equivalent of T299, is found in a carcinoma (*49*). This mutation would disrupt the start of the long helix. Q324L (*50*), which is the merlin equivalent of Q308, would disrupt the hydrogen bond to R40 on domain F1. L339F, which is the equivalent of L323 in moesin, is found in a sporadic meningioma (*51*). L323 is quite solvent exposed and forms part of the hydrophobic surface of the helix. The pathogenic replacement by Phe would indicate that the size of this residue is important, supporting the involvement of the helix in packing against other residues in the full protein.

Sequence analysis of the α-region (residues 300−470) of ERM proteins (*12*) predicted formation of coiled coils (*51*) and a helical dimer (*12*). As the contact between the ERMAD is a head-to-tail association, the coiled coil would be antiparallel in either a heterodimer or a dormant monomer (Figure 1). If a dormant monomer is to be formed by head-to-tail association of the N- and C-ERMADs, the helix seen in this structure must terminate and turn back on itself (Figure 1). Calculated breaks in the helices are predicted at residues 357, 409−414, and 441 and clearly at residue 469 using Coils2 (*52*). This predicts a pair of helices of ∼54 residues and a pair of helices of ∼28 residues.

One of the crystal contacts is between the long helices in symmetry-related molecules. The main hydrophobic interaction is between M318 and M322, but there is also a salt bridge between residues R320 and E324 and a hydrogen bond from R320 to N325. This combination of hydrophobic interactions and salt bridges is typical of the type of interactions found in coiled coils. However, the angle between the two helices is much larger than the value of 20° in a classic coiled coil (*52*), so these helices do not make an extended contact. Nevertheless, there is a helical hydrophobic surface similar to that of other dimeric coiled coils such as the adenomatous Polyposis coli Protein (1DEB) (*53*) or colicin Ia (1CII) (*54*), supporting the coiled-coil prediction.

Changes to the C-ERMAD Binding Region on Activation. The main part of the C-ERMAD sits across domains F2 and F3 (Figure 2a). Residues 260−265 in our unliganded structure would be clashing with the C-terminus of the

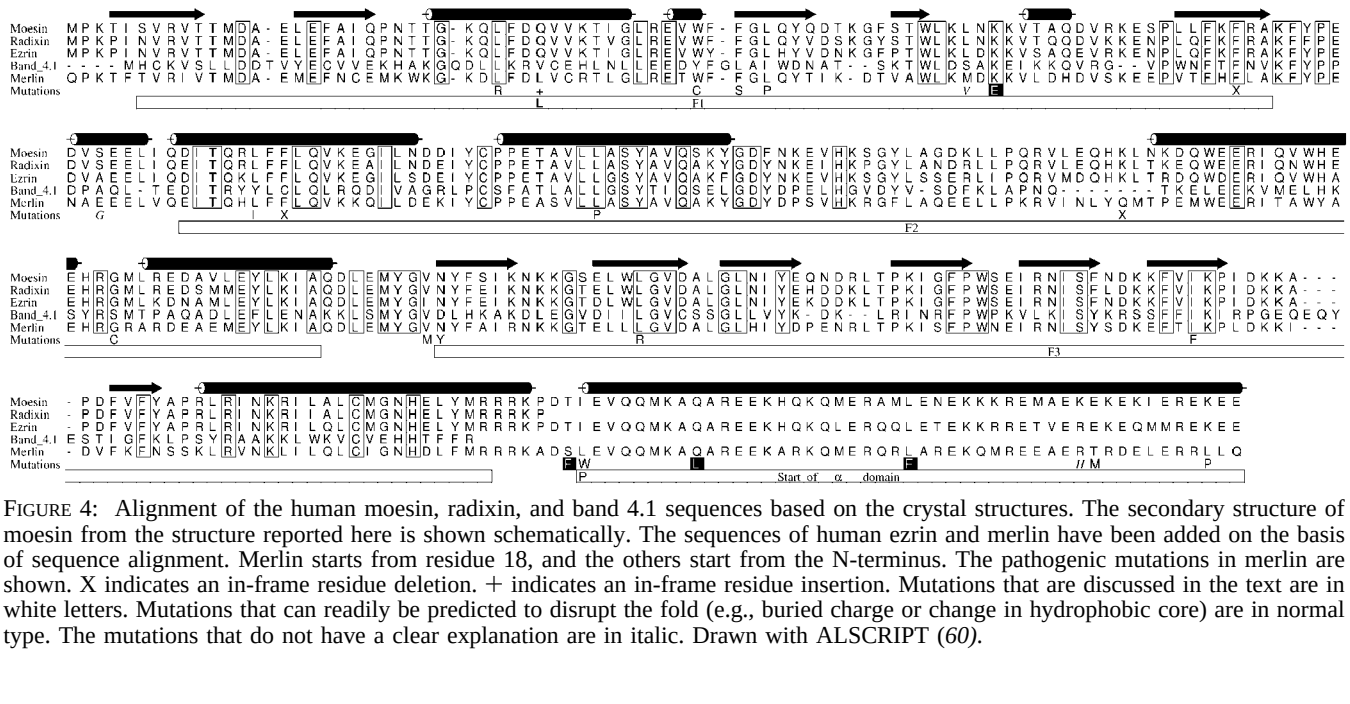

FIGURE 4: Alignment of the human moesin, radixin, and band 4.1 sequences based on the crystal structures. The secondary structure of moesin from the structure reported here is shown schematically. The sequences of human ezrin and merlin have been added on the basis of sequence alignment. Merlin starts from residue 18, and the others start from the N-terminus. The pathogenic mutations in merlin are shown. X indicates an in-frame residue deletion. + indicates an in-frame residue insertion. Mutations that are discussed in the text are in white letters. Mutations that can readily be predicted to disrupt the fold (e.g., buried charge or change in hydrophobic core) are in normal type. The mutations that do not have a clear explanation are in italic. Drawn with ALSCRIPT (*60*).

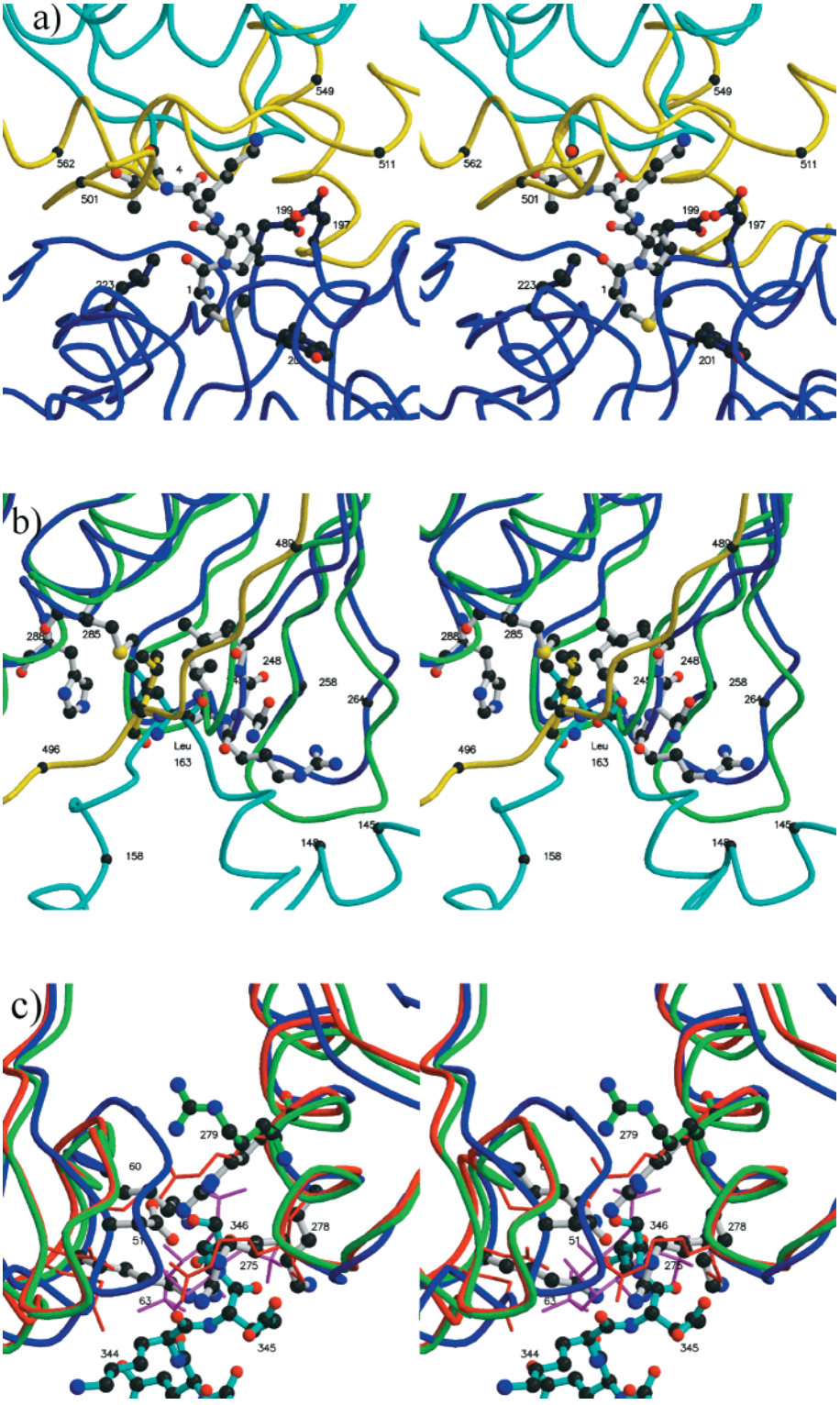

FIGURE 5: Stereopairs of regions discussed in the text. (a) Interaction of the N-terminus with an adjacent FERM domain. The two interacting activated moesin chains are in cyan and blue. The four N-terminal residues (gray) and the principal interacting residues (blue) are shown as ball-and-stick models. The position of the C-ERMAD in the structure of Pearson et al. (*33*) is shown in yellow, demonstrating that it would block this site in the dormant complex. (b) Interaction of the loops of residues 159−165 (cyan from one active moesin chain) and 260−264 (blue from the second active moesin chain) in the crystal contact. The C-ERMAD backbone is in yellow and the FERM domain in green from the superimposed dormant moesin complex. Leucine 163 from moesin residues 1−346 (cyan) and leucine 494 (yellow) from the first strand of the C-ERMAD in the dormant complex (*33*) are shown as ball-and-stick models. Residues in contact with Leu 163 in the other chain are also shown as ball-and-stick models (gray). (c) Interaction of the C-terminus of the long α-helix of one active moesin molecule (cyan) with the FERM domain of another activated moesin domain in blue. The superimposed dormant FERM domain is in green and the IP3-bound radixin in red. The IP3 molecule is drawn as bonds in purple showing it overlaps with the C-terminal side chain. Side chains interacting with the C-terminus are shown as gray ball-and-stick models. The equivalent radixin side chains are in red bonds. R279 of the dormant FERM domain is in green showing its different conformation. All figures drawn with MOLSCRIPT (*57*) and Raster3D (*58*).

C-ERMAD in the region of Thr 566 if the C-ERMAD was present. The radixin structures resemble our activated structure in this region. In our moesin structure, residues 258−264 form a crystal contact with residues 159−165, but this contact is not present in the radixin structures, suggesting that crystal contacts alone are not causing this difference. Therefore, one consequence of removing the C-ERMAD is to alter the position of the loop of residues 260−264. It was suggested by Hamada et al. (*34*) that this change is a result of IP3 binding, and this is how PIP2 activates ERM proteins by causing this loop to move and displacing the C-ERMAD. Since fairly similar changes are seen in the radixin structure without IP3, the radixin structure with IP3, and the active moesin structure, where there may be activation by a negatively charged peptide (see below), it is difficult to conclude that this conformation is caused by changes elsewhere in the molecule rather than just by the absence of the C-ERMAD.

The helix of residues 165−176 of F2 in active moesin has moved toward the position that would be occupied by the C-ERMAD as reported by Hamada et al. (*34*) for radixin. This is despite large differences in the loop of residues 160−164 between radixin and active moesin caused by the crystal contact in the active moesin structure. The adjacent loop consisting of residues 139−148 that packs against the other side of the helix moves in the radixin and active moesin structures in concert with the helix.

The crystal contact with the N-terminus of another moesin would not be possible in the presence of the C-ERMAD. The N-terminal methionine is inserted toward the core of the FERM domain so that it contacts both the linkers between F1 and F2 (residues 85−87) and between F2 and F3 (residues 196−203) and parts of F3 (residues 221−228). This binding pocket would be blocked by the 3_{10}-helix and helix C of the C-ERMAD in the dormant complex (Figure 5a). The N-terminal methionine is much deeper in this cleft than any part of the C-ERMAD. It is unlikely that this is a physiological interaction between FERM domains as the N-terminal methionine, which forms a large part of this interface, is not present in moesin as isolated from HL-60 cells (*6*). Nevertheless, this pocket used in the crystal contact may be part of the binding interface for some of the partners of the FERM domain.

The first strand of the C-ERMAD (residues 488−494) is domain swapped in the dormant structure (*33*) and lies on the edge of one of the β-sheets of domain F3. In the fourth crystal contact, leucine 163 in our structure superimposes with leucine 494 in strand 1 of the C-ERMAD (Figure 5b) and forms similar contacts to amino acids 245−248, 285, and 288. This is another possible binding region exposed on removal of the C-ERMAD.

Inositol Binding Region. Inositol lipids, particularly phosphatidylinositol 4,5-bisphosphate (PIP2), have been shown to enhance CD44 binding. The binding site has been defined in radixin crystals containing inositol 1,4,5-trisphosphate (IP3) (*34*) and independently by mutagenesis in ezrin (*55*). It lies in a positively charged cleft between domains F1 and F3. The C-terminus of our moesin construct is highly charged (REKEE) and interacts with this cleft. The carboxylic group of the glutamic side chain lies exactly where IP3 binds in the radixin structure (Figure 5c). The negatively charged residues and the C-terminal carboxyl interact with a positively charged patch at the start of the helix of module F3 (R275, K278, and R279) and K60 and K63 of module F1. Most of these residues bind to IP3 in the radixin structure. It is unlikely therefore that IP3 would bind to our crystal form. The K79E mutation in merlin (equivalent to K63 in moesin) is pathogenic, further emphasizing the importance of the basic residues in this region.

The interaction with the negatively charged peptide causes greater structural changes than IP3 binding. In our structure, the outer part of domain F1 (residues 49−57 and 66−76) moves toward domain F3 relative to the position in the dormant structure and in the radixin structure. As R275 which interacts with D51 in the other structures is interacting with the C-terminus, D51 instead forms a hydrogen bond to R279 which requires the loop to move about 4.5 Å (Figures 2a and 5c) which propagates through much of domain 1.

It is an intriguing observation that a negatively charged peptide causes an even greater structural shift than a proven physiological activator. One of the most well-known examples of a negatively charged C-terminus is that of tubulin subunits, although these are disordered in the electron diffraction structures (*56*). Whether the negatively charged peptide interaction has any physiological role has not yet been tested.

SUMMARY AND CONCLUSION

The structure of the activated FERM domain of moesin presented here allows a direct comparison with the dormant FERM domain/C-ERMAD complex of moesin (*33*). Further comparison with the isolated radixin FERM domain, which has different crystal contacts, allows us to identify those regions which shift consistently in the absence of the C-ERMAD. These are the loop of residues 260−264 in subdomain F3 and the helix of residues 166−170 in domain F2. These changes propagate through adjacent pieces of structure.

Intriguingly in a crystal contact, a negatively charged peptide occupies the inositol binding site and causes a larger shift in domain F1 than is seen on inositol binding. The physiological relevance of this has not yet been tested.

The structure also contains a long helix at the start of the α-domain. This confirms the secondary structure prediction and defines the position of this domain relative to the FERM domain. It also allows the interpretation of a number of pathogenic mutations in the related tumor suppressor merlin.

ACKNOWLEDGMENT

We thank Prof. P. Mangeat and Dr. Richard Lamb for the full-length moesin−GST construct. We thank the protein crystallography staff at Daresbury and Hamburg for data collection facilities, particularly James Nicholson and Wojtek Rypniewski. The data collection at Hamburg was supported by European Community-Access to Research Infrastructure Action of the Improving Human Potential Programme to the EMBL Hamburg Outstation, Contract HPRI-CT-1999−00017.

REFERENCES

1. Bretscher, A. (1999) *Curr. Opin. Cell Biol. 11*, 109−116.
2. Mangeat, P., Roy, C., and Martin, M. (1999) *Trends Cell Biol. 9*, 187−192.

3. Tsukita, S., Yonemura, S., and Tsukita, S. (1997) *Trends Biochem. Sci. 22*, 53−58.
4. Bretscher, A. (1983) *J. Cell Biol. 97*, 425−432.
5. Tsukita, S., Heida, Y., and Tsukita, S. (1989) *J. Cell Biol. 108*, 2369−2382.
6. Lankes, W., and Furthmayr, H. (1991) *Proc. Natl. Acad. Sci. U.S.A. 88*, 8297−8301.
7. Trofatter, J. A., MacCollin, M. M., Rutter, J. L., Murrell, J. R., Duyao, M. P., Parry, D. M., Eldridge, R., Kley, N., Menon, A. G., Pulaski, K., Haase, V. H., Ambrose, C. M., Munroe, D., Bove, C., Haines, J. L., Martuza, R. L., MacDonald, M. E., Seizinger, B. R., Short, M. P., Buckler, A. J., and Gusella, J. F. (1993) *Cell 72*, 791−800.
8. Evans, D. G. R., Sainio, M., and Base, M. E. (2000) *J. Med. Genet. 37*, 897−904.
9. Anderson, R. A., and Lovrien, R. E. (1984) *Nature 307*, 655−658.
10. Chishti, A. H., Kim, A. C., Marfatia, S. M., Lutchman, M., Hanspal, M., Jindal, H., Liu, S. C., Low, P. S., Rouleau, G. A., Mohandas, N., Chasis, J. A., Conboy, J. G., Gascard, P., Takakuwa, Y., Huang, S. C., Benz, E. J., Bretscher, A., Fehon, R. G., Gusella, J. F., Ramesh, V., Solomon, F., Marchesi, V. T., Tsukita, S., Tsukita, S., Arpin, M., Louvard, D., Tonks, N. K., Anderson, J. M., Fanning, A. S., Bryant, P. J., Woods, D. F., and Hoover, K. B. (1998) *Trends Biochem. Sci. 23*, 281−282.
11. Giarault, J. A., Labesse, G., Mornon, J. P., and Callebaut, I. (1999) *Trends Biochem. Sci. 24*, 54−57.
12. Turunen, O., Sainio, M., Jaaskelainen, J., Carpen, O., and Vaheri A. (1998) *Biochim. Biophys. Acta 1387*, 1−16.
13. Turunen, O., Wahlstrom, T., and Vaheri, A. (1994) *J. Cell Biol. 126*, 1445−1453.
14. Roy, C., Martin, M., and Mangeat, P. (1997) *J. Biol. Chem. 272*, 20088−20095.
15. Martin, M., Roy, C., Montcourrier, P., Sahuquet, A., and Mangeat, P. (1997) *Mol. Cell. Biol. 8*, 1543−1557.
16. Winder, S. J., Knight, A. E., and Kendrick-Jones, J. (1997) in *Dystrophin, genetics, protein and cell biology* (Brown, S. C., and Lucy, J. A., Eds.) Cambridge University Press, Cambridge, U.K., pp 27−55.
17. Moores, C. A., Keep, N. H., and Kendrick-Jones, J. (2000) *J. Mol. Biol. 297*, 465−480.
18. Gary, R., and Bretscher, A. (1995) *Mol. Biol. Cell 6*, 1061−1075.
19. Nakamura, F., Amieva, M. R., and Furthmayr, H. (1995) *J. Biol. Chem. 270*, 31377−31385.
20. Matsui, T., Maeda, M., Doi, Y., Yonemura, S., Amano, M., Kaibuchi, K., Tsukita, S., and Tsukita, S. (1998) *J. Cell Biol. 140*, 647−657.
21. Tsukita, S., Oishi, K., Sato, N., Sagara, J., Kawai, A., and Tsukita, S. (1994) *J. Cell Biol. 126*, 391−401.
22. Yonemura, S., Hirao, M., Doi, Y., Takahashi, N., Kondo, T., Tsukita, S., and Tsukita, S. (1998) *J. Cell Biol. 140*, 885−895.
23. Legg, J. W., and Isacke, C. M. (1998) *Curr. Biol. 8*, 705−708.
24. Niggli, V., Andreoli, C., Roy, C., and Mangeat, P. (1995) *FEBS Lett. 376*, 172−176.
25. Hirao, M., Sato, N., Kondo, T., Yonemura, S., Monden, M., Sasaki, T., Takai, Y., Tsukita, S., and Tsukita, S. (1996) *J. Cell Biol. 135*, 37−51.
26. Heiska, L., Alfthan, A., Gronholm, M., Vilija, P., Vaheri, A., and Carpen, O. (1998) *J. Biol. Chem. 273*, 21893−21900.
27. Reczek, D., and Bretscher, A. (1998) *J. Biol. Chem. 273*, 18452−18458.
28. Gautreau, A., Poullet, P., Louvard, D., and Arpin, M. (1999) *Proc. Natl. Acad. Sci. U.S.A. 96*, 7300−7305.
29. Yun, C. H. C., Lamprecht, G., Forster, D. V., and Sidor, A. (1998) *J. Biol. Chem. 273*, 25856−25863.
30. Takahashi, K., Sasaki, T., Mammoto, A., Takaishi, K., Kameyama, T., Tsukita, S., Tsukita, S., and Takai, Y. (1997) *J. Biol. Chem. 272*, 23371−23375.
31. Takahashi, K., Sasaki, T., Mammoto, A., Hotta, I., Takaishi, K., Imamura, H., Nakano, K., Kodama, A., and Takai, Y. (1998) *Oncogene 16*, 3279−3284.
32. Fukata, Y., Kimura, K., Oshiro, N., Saya, H., Matsuura, Y., and Kaibuchi, K. (1998) *J. Cell Biol. 141*, 409−418.
33. Pearson, M. A., Reczek, D., Bretscher, A., and Karplus, P. A. (2000) *Cell 101*, 259−270.
34. Hamada, K., Shimizu, T., Matsui, T., Tsukita, S., Tsukita, S., and Hakoshima, T. (2000) *EMBO J. 19*, 4449−4462.
35. Leslie, A. (1993) in *Proceedings of the CCP4 Study Weekend, January 29−30. 1993* (Sawyer, L., Issac, N., and Bailey, S., Eds.) pp 44−51, Daresbury Laboratory, Warrington, U.K.
36. Collaborative Computational Project, No. 4. (1994) *Acta Crystallogr. D50*, 760−763.
37. Evans, P. (1997) In *Proceedings of the CCP4 Study Weekend, January 29−30. 1997* (Sawyer, L., Issac, N., and Bailey, S., Eds.) Daresbury Laboratory, Warrington, U.K.
38. Terwilliger, T. C., and Berendzen, J. (1999) *Acta Crystallogr. D55*, 849−861.
39. La Fortelle, E., and Bricogne, G. (1997) *Methods Enzymol. 276*, 472−494.
40. Jones, T. A., Zou, J. Y., Cowan, S. W., and Kjelgaard, M. (1991) *Acta Crystallogr. A47*, 110−119.
41. Brünger, A. T., Adams, P. D., Clore, G. M., DeLano, W. L., Gros, P., Grosse-Kunstleve, R. W., Jiang, J. S., Kuszewski, J., Nilges, M., Pannu, N. S., Read, R. J., Rice, L. M., Simonson, T., and Warren, G. L. (1998) *Acta Crystallogr. D54*, 905−921.
42. Guex, N., and Peitsch, M. C. (1997) *Electrophoresis 18*, 2714−2723.
43. Hayward, S., and Berendsen, H. J. C. (1998) *Proteins 30*, 144−154.
44. Krawczak, M., and Cooper, D. N. (1997) *Trends Genet. 13*, 121−122.
45. Han, B., Nunomura, W., Takakuwa, Y., Mohandas, N., and Jap, B. K. (2000) *Nat. Struct. Biol. 7*, 871−875.
46. Vijay-Kumar, S., Bugg, C. E., and Cook, W. J. (1987) *J. Mol. Biol. 194*, 531−544.
47. Kragelund, D. D., Anderson, K. V., Madsen, J. C., Knudsen, J., and Poulsen, F. M. (1993) *J. Mol. Biol. 230*, 1260−1277.
48. Forman-Kay, J. D., and Pawson, T. (1999) *Curr. Opin. Struct. Biol. 9*, 690−695.
49. Arakawa, H., Hayashi, N., Nagase, H., Ogawa, M., and Nakamura, Y. (1994) *Hum. Mol. Genet. 3*, 565−568.
50. Wellenreuther, R., Kraus, J. A., Lenartz, D., Menon, A. G., Schramm, J., Louis, D. N., Ramesh, V., Gusella, J. F., Wiestler, O. D., and Vondeimling, A. (1995) *Am. J. Pathol. 146*, 827−832.
51. DeVitis, L. R., Tedde, A., Vitelli, F., Ammannati, F., Mennonna, P., Bigozzi, U., Montali, E., and Papi, L. (1996) *Hum. Genet. 97*, 632−637.
52. Lupas, A., Van Dyke, M., and Stock, J. (1991) *Science 252*, 1162−1164.
53. Day, C. L., and Alber, T. (2000) *J. Mol. Biol. 301*, 147−156.
54. Wiener, M., Freymann, D., Ghosh, P., and Stroud, R. M. (1997) *Nature 385*, 461−465.
55. Barret, C., Roy, C., Montcourrier, P., Mangeat, P., and Niggli, V. (2000) *J. Cell Biol. 151*, 1067−1079.
56. Nogales, E., Wolf, S. G., and Downing, K. H. (1998) *Nature 391*, 199−202.
57. Kraulis, P. J. (1991) *J. Appl. Crystallogr. 24*, 946−950.
58. Merritt, E. A., and Bacon, D. J. (1997) *Methods Enzymol. 277*, 505−524.
59. Kleywegt, G. J. (1996) *Acta Crystallogr. D52*, 842−857.
60. Barton, G. J. (1993) *Protein Eng. 6*, 37−40.

BI010419H